Available online at www.sciencedirect.com

SciVerse ScienceDirect

Procedia Technology 7 (2013) 118 – 125

Procedia Technology

Blind Decomposition of Multi-spectral Fluorescence Lifetime Imaging Microscopy Data: Further Validation

O. Gutierrez-Navarro[a,*], Daniel U. Campos-Delgado[a], E. R. Arce-Santana[a], M. O. Mendez[a], Javier A. Jo[b]

[a]*Facultad de Ciencias, Universidad Autonoma de San Luis Potosi, Av. Salvador Nava s/n, Zona Universitaria, 78290, San Luis Potosi, Mexico.*

[b]*Department of Biomedical Engineering, Texas A&M University, 5045 Emerging Technologies Building, College Station, TX 77843-3120, USA*

Abstract

Characterization of living tissue without the need for biopsies is the goal of several probe technologies such as Multi-spectral Fluorescence Lifetime Imaging Microscopy. This technique measures the mixed response from the endogenous fluorophores within an organic sample. This response is decomposed into the individual response from every constituent using a fully constrained linear unmixing algorithm: Blind End-member and Abundance Extraction (BEAE). Further validation of the method is needed specially when dealing with real laboratory samples. Moreover, the BEAE method incorporates a regularization parameter during the quadratic optimization procedure which has to be tuned to improve the estimation accuracy. Different values for the regularization parameter are tested using synthetic data at a signal-to-noise ratio of 10 dB and 15 dB. The relative error against the ideal end-members for each component is measured. Results show that the estimation accuracy in each end-member increases when the regularization parameter is around 0.75. Blind decomposition of m-FLIM data from coronary samples is also performed for validation purposes. The extracted fluorescence decays are identified as collagen, elastin and LDL responses. Histopatology slides are used as reference to validate the results. Synthetic simulation shows that the BEAE algorithm performs a more accurate estimation of the end-members profiles due to the regularization term. Furthermore, analysis performed on ex-vivo samples match the qualitative description provided by histopatology slides.

Selection and peer-review under responsibility of CIIECC 2013

Keywords: Blind End-member Decomposition, Linear Spectral Unmixing, Multi-spectral Fluorescence Lifetime Imaging Microscopy, Regularization, Autofluorescence

1. Introduction

Fluorescence Lifetime Imaging Microscopy [1, 2, 3, 4] (FLIM) is a technology that aims to provide painless and minimally invasive characterization of living tissue. FLIM data measures the fluorescence intensity decay from a sample in different wavelength bands, namely 390 ± 20 nm, 452 ± 22.5 nm and

*Corresponding author. Tel. +52 (444) 8262491 ext. 2903

Email addresses: omargn@gmail.com (O. Gutierrez-Navarro), ducd@fciencias.uaslp.mx (Daniel U. Campos-Delgado), arce@fciencias.uaslp.mx (E. R. Arce-Santana), mmendez@fc.uaslp.mx (M. O. Mendez), javierjo@bme.tamu.edu (Javier A. Jo)

Selection and peer-review under responsibility of CIIECC 2013

doi:10.1016/j.protcy.2013.04.015

550±20 nm. These measurements contain the mixed response emitted by endogenous fluorescent molecules contained in the imaged sample. Meaningful data is obtained by decomposing multi-spectral-FLIM (m-FLIM) measurements into the fluorescence intensity decay from each constituent component (end-members) and their proportional concentrations [5, 6, 7].

The Linear mixture model [8, 9] states that fluorescence decay mixtures $y_{k,\lambda}(t)$ are a linear combination of the fluorescence decay $p_{n,\lambda}(t)$ and fractional contributions (abundances) $\alpha_{k,n}$ of each end-member. Given a spatial position k and wavelength λ, over $t = 1, \ldots, T$ time samples, the mixture data is modelled as

$$y_{k,\lambda}(t) = \sum_{n=1}^{N} \alpha_{k,n} p_{n,\lambda}(t) \qquad \forall k = 1, \ldots, K, \ \& \ \lambda = 1, \ldots, W, \tag{1}$$

where K represents the total number of spatial measurements, N the number of end-members in the sample, and W the number of wavelengths used in the experiment. The expression in (1) be rewritten in matrix notation as

$$\boldsymbol{Y} = [\mathbf{y}_1, \ldots, \mathbf{y}_K] = \underbrace{[\mathbf{p}_1, \ldots, \mathbf{p}_N]}_{\mathbf{P}} \underbrace{[\boldsymbol{\alpha}_1, \ldots, \boldsymbol{\alpha}_K]}_{\mathcal{A}} \tag{2}$$

where $\mathbf{y}_{k,\lambda} = [y_{k,\lambda}(1) \ \ldots \ y_{k,\lambda}(T)]^T$ contains all the measurements available at spatial location k and wavelength λ, $\mathbf{p}_{n,\lambda} = [p_{n,\lambda}(1) \ \ldots \ p_{n,\lambda}(T)]$ defines a vector of the n-th end-member at wavelength λ. Meanwhile $\mathbf{p}_n = [\mathbf{p}_{n,1}^T \ \ldots \ \mathbf{p}_{n,W}^T]^T$ and $\boldsymbol{\alpha}_k = [\alpha_{k,1}, \cdots, \alpha_{k,N}]^T$ stand for the end-embers and their abundances for the n component and k spatial location, respectively. Finally, $\mathbf{y}_k = [\mathbf{y}_{k,1}^T \ \ldots \ \mathbf{y}_{k,W}^T]^T$ the overall measurement vector at k spatial location, and define its length as $D = W \cdot T$.

2. Blind End-member and Abundance Extraction

Given the measurements $\mathbf{Y} \in \mathbb{R}^{D \times K}$ from the m-FLIM data, the blind end-member decomposition problem [10, 11, 12] consists of estimating the end-member profiles $\mathbf{P} \in \mathbb{R}^{D \times N}$ and their corresponding abundance $\mathcal{A} \in \mathbb{R}^{N \times K}$ under component-wise non-negativity and sum-to-one constraints. The complete linear unmixing problem for m-FLIM data can be written as:

$$\min_{\mathbf{P},\mathcal{A}} \frac{1}{2} \|\boldsymbol{Y} - \mathbf{P}\mathcal{A}\|_F^2 \tag{3}$$

such that

$$\boldsymbol{\alpha}_k^T \mathbf{1}_N = \sum_{n=1}^{N} \alpha_{k,n} = 1 \qquad \forall k \tag{4}$$

$$\alpha_{k,n} \geq 0 \qquad \forall k, n \tag{5}$$

$$\mathbf{p}_n^T \mathbf{1}_D = \sum_{\lambda=1}^{W} \sum_{t=1}^{T} p_{n,\lambda}(t) = 1 \qquad \forall n \tag{6}$$

$$p_{n,\lambda}(t) \geq 0 \qquad \forall n, \lambda, t, \tag{7}$$

where $\|\mathbf{B}\|_F = \sqrt{\text{Trace}\left(\mathbf{B}^T\mathbf{B}\right)}$ is the Frobenius norm, and $\mathbf{1}_X$ is a vector filled with ones of dimension X.

The Blind End-member and Abundance Extraction (BEAE) method [13] for m-FLIM data proposes to solve at one step for the end-member profiles by the following quadratic optimization problem:

$$\min_{\mathbf{P} \geq 0} \mathbf{J} = \min_{\mathbf{P} \geq 0} \frac{1}{2} \|\mathbf{Y} - \mathbf{P}\mathcal{A}\|_F^2 + \boldsymbol{\chi}^T \left(\mathbf{P}^T \mathbf{1}_D - \mathbf{1}_N\right) + \rho \text{Trace}\left\{\mathbf{POP}^T\right\} \tag{8}$$

where $\boldsymbol{\chi} \in \mathbb{R}^N$ is a vector of Lagrange multipliers associated to the sum-to-one constraint in 6, and $\mathbf{O} = N\mathbf{I}_N - \mathbf{1}_N\mathbf{1}_N^T$ is a symmetric matrix related to teh regularization term. The BEAE method provides a closed-form solution to estimate the end-member profiles given by

$$\mathbf{P} = \left(\mathbf{I}_D - \frac{1}{D}\mathbf{1}_D\mathbf{1}_D^T\right)\mathbf{Y}\mathcal{A}^T\left(\mathcal{A}\mathcal{A}^T + \rho\mathbf{O}\right)^{-1} + \frac{1}{D}\mathbf{1}_D\mathbf{1}_N^T \tag{9}$$

where $\mathbf{I}_D$ represents the identity matrix of D order.

The idea behind BEAE is to estimate the end-members by (9) and the abundances by using the constrained optimization (CO) approach in [14], in an alternating least squares [15] fashion. The overall iterative methodology is reproduced in Algorithm 1.

Algorithm 1: Alternating Least Squares Procedure for Blind End-member and Abundance Extraction on m-FLIM data

Given the number of components N, the m-FLIM mixture data in matrix $\boldsymbol{Y}$ and a tolerance parameter ϵ.

1. Initialize the end-members matrix $\mathbf{P}^0$ according to a priori knowledge, for example randomly selecting N linearly independent measurements from $\boldsymbol{Y}$, or by the singular value decomposition (SVD) of $\boldsymbol{Y}$ [11]. Verify that the selected initial end-members $\mathbf{P}^0$ satisfy the sum-to-one constraint and non-negativity constraints in (6) and (7).
2. Estimate the optimal fractional concentrations $\mathcal{A}^{i+1}$ by using the CO Algorithm in [14], taking $\mathbf{P}^i$ and N as input data.
3. Calculate the optimal end-members matrix $\mathbf{P}^{i+1}$ by using the closed-form solution in (9) with $\mathcal{A}^{i+1}$ as input term.
4. Check for negative elements in matrix $\mathbf{P}^{i+1}$. If any, project them to zero and re-normalize each column in $\mathbf{P}^{i+1}$.
5. Check for convergence of the optimal cost function in (8), if the decrement is not lower than a threshold ϵ continue to the next iteration and go to step 2), otherwise stop the iteration.

In the resulting optimal solution of (9), the regularization parameter ρ plays an important role, since it affects the inverse of a matrix. In [13], the impact of this term on the optimal end-members was not analysed in detail. In this way, the next section presents an evaluation of this parameter with respect to the estimation accuracy of the end-members for a synthetic scenario.

3. Influence of the Regularization Parameter

In this section, we study how the performance of BEAE is affected by the regularization parameter ρ. Computer simulations are performed using synthetic m-FLIM datasets build up from the fluorescence intensity decays of collagen, elastin and low density lipoproteins (LDL); obtained from [16]. A synthetic abundance map designed to represent a highly mixed scenario is employed to generate the synthetic m-FLIM dataset. The simulated concentrations are displayed in the top panel of Figure 1, the abundance map obtained from a single experiment is shown in the lower panel. The corresponding end-member profiles are displayed in Figure 2. The projection of the data and end-members into a lower dimensional subset is helpful to appreciate the quality of the estimation, as can be seen in Figure 3. These results were obtained from a synthetic m-FLIM dataset with a SNR of 15 dB and $\rho = 0.75$.

The regularization parameter in the cost function (8) is designed to penalize the distance between the vertices of the N-dimensional simplex [17, 18]. If the regularization helps to improve the solution, then it should be noticed in the estimation of the end-members. In addition, the mixtures produced along with the extracted abundances should better explain the m-FLIM data under the constrains (4) to (7).

In order to illustrate the dependence of the estimation accuracy on the regularization term, a new evaluation was conducted using different values for ρ, from 0 to 20. For each experiment, white Gaussian noise was added to the synthetic m-FLIM datasets, achieving a SNR of 10 dB and 15 dB. The noisy m-FLIM datasets were later decomposed into end-members and their abundances using Algorithm 1. Twenty simulations were performed for each value of ρ.

A percent relative error (PRE) is employed to measure the effect on the solution provided by the BEAE

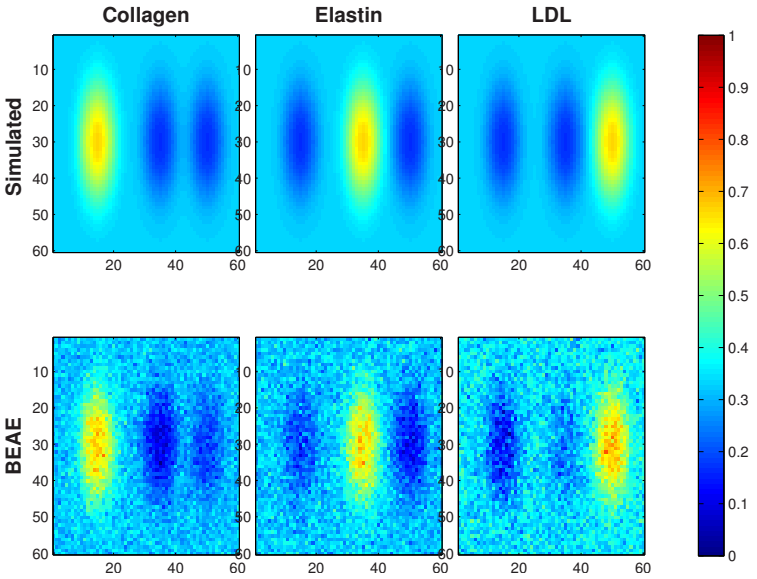

Fig. 1. The top row shows the simulated abundance map, in a noise free scenario. White Gaussian noise was added for a signal-to-noise ratio of 15 dB. The abundance map obtained using Algorithm 1 is displayed in the lower row for each component. This result was obtained using $\boldsymbol{\rho} = 0.75$

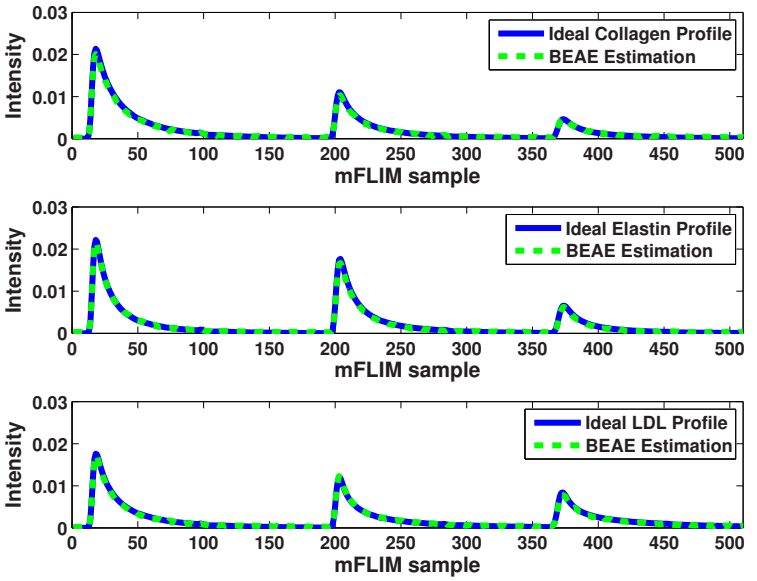

Fig. 2. Comparison between the ideal profiles (collagen, elastin and LDL) and the end-member profiles extracted from a synthetic m-FLIM data set using the BEAE Algorithm. This data was obtained from an experiment with SNR = 15 dB and $\rho = 0.75$

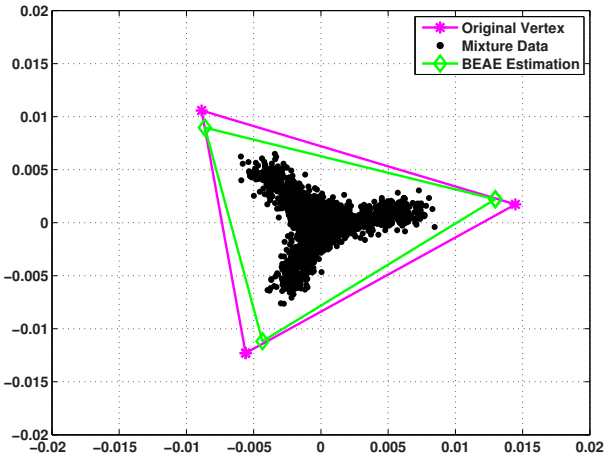

Fig. 3. The m-FLIM dataset and extracted end-members projected into a 2-dimensional subset using Principal Component Analysis for dimensional reductions. The blindly extracted components (green vertex) in this experiment are extremely close to the ideal end-members (magenta vertex). As can be seen, the estimation encloses the projected data (black points) and therefore satisfies the constraints in equations (4) and (5). This data was obtained from an experiment with SNR = 15 dB and $\rho = 0.75$.

algorithm, this error is defined as

$$\mathrm{E}_n = 100 \times \frac{\|\mathbf{p}_n - \widehat{\mathbf{p}}_n\|_2^2}{\|\mathbf{p}_n\|_2^2} \qquad \forall n = 1, \ldots, N, \tag{10}$$

where $\mathbf{p}_n$ is the ideal end-member profile and $\widehat{\mathbf{p}}_n$ is the corresponding profile extracted by the BEAE Algorithm. The average PRE obtained in the simulations, with a SNR of 10 dB and 15 dB, is shown in Figures 4 and 5.

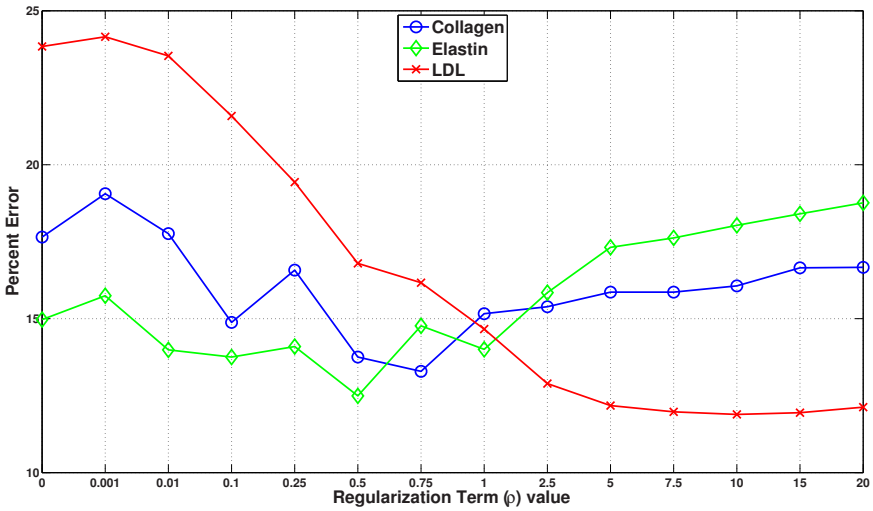

Fig. 4. Average PRE of the estimated end-members collagen, elastin and LDL for SNR = 10 dB

These results illustrate the importance of selecting correctly the value of ρ, since for small or large

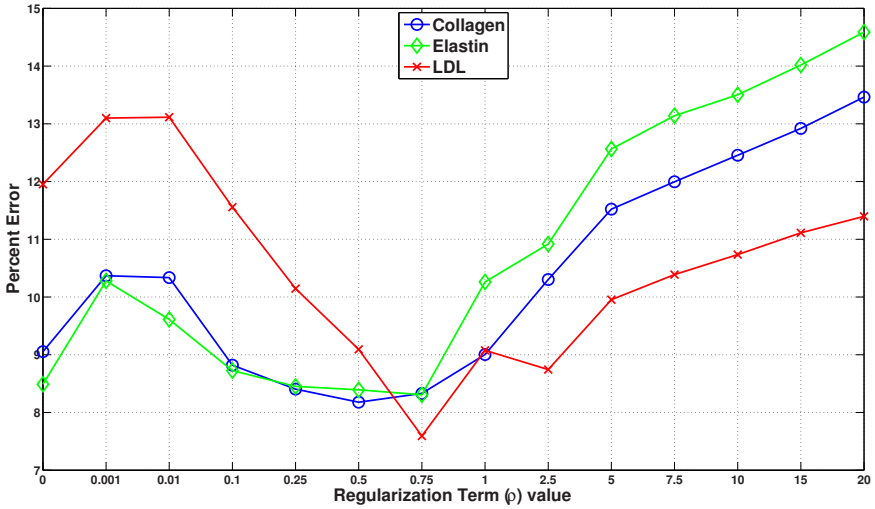

Fig. 5. Average PRE of the estimated end-members collagen, elastin and LDL for SNR = 15 dB

regularization terms, the accuracy is clearly sacrificed. In this way, for SNR of 10 dB and 15 dB, the best trade-off is found for $\rho = 0.75$, although a value in the interval $0.1 \leq \rho \leq 1$ achieves satisfactory results.

4. Decomposition of Experimental Samples

End-member decomposition and abundance extraction of experimental m-FLIM datasets is performed to provide quantitative characterization of living tissue. The synthetic experiments have been successful but the BEAE algorithm must be able to provide solutions with biologically plausible solutions when dealing with real samples.To test a real case scenario, three m-FLIM datasets were used to evaluate the BEAE algorithm. These datasets were sampled from fresh post-mortem human coronary plaques, obtained from [19].

Additionally, histological sections from the post-mortem samples were taken in order to provide a qualitative reference. The abundance maps obtained are shown in Figure 6. The histopathology slides were taken from the cross-section of the imaged samples, indicated by dotted black lines in the abundance maps. The sample in the top row depicts regions with localized concentrations of collagen, elastin and LDL. The histopatology slide also reflects a complex scenario with the presence of three fluorophores.

The second specimen (middle section in Figure 6) portraits a tissue sample rich in elastin and LDL, two sections corresponding to each auto-fluorescent molecule are shown in the abundance map; its corresponding histopathology shows different regions dominated by elastin on the right, and lipids on the left side of the sample. Some collagen rich regions are also detected in the central region of the sample.

Histopathology from the third sample (bottom panel in Figure 6) shows regions rich in elastin and collagen. The abundance maps calculated certainly indicates two different regions with a high proportional concentration of collagen and elastin in the lower and upper sections, respectively. Small amounts of LDL are also detected by the BEAE algorithm.

5. Discussion and Final Remarks

Experimental results show that the regularization parameter is helping the estimation of the end-member profiles. The BEAE algorithm [13] performs the best when using a lower value for $\boldsymbol{\rho}$, in the interval 0.1 to 1.0. Moreover, the histopatology slides from the ex-vivo samples confirms that the qualitative description from BEAE provides a good characterization of organic samples.

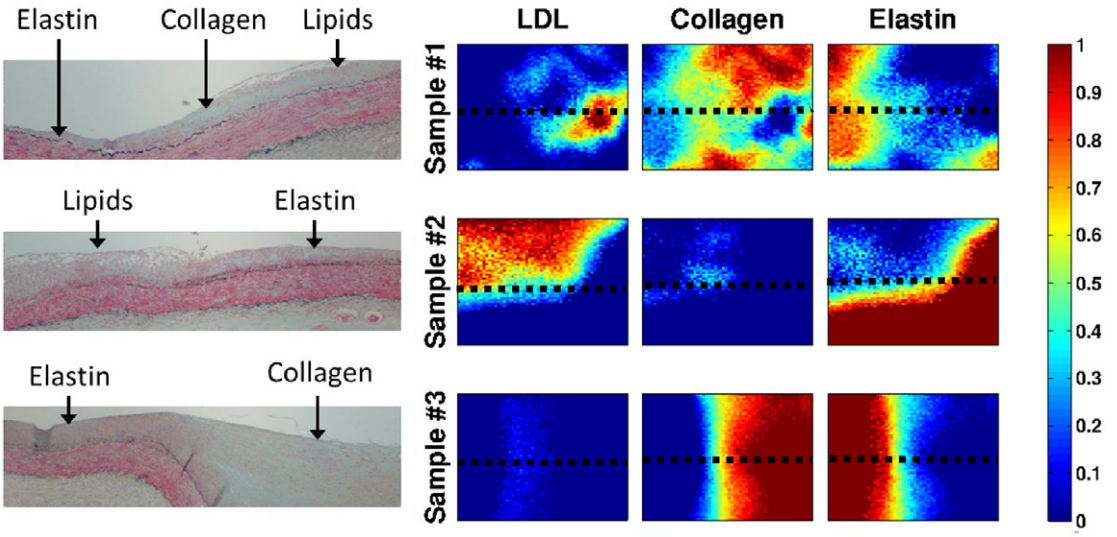

Fig. 6. Representative histopathology slides (left panels) and estimated abundance maps (right panels) from three coronary samples with high content of three endogenous fluorophores: collagen, elastin and LDL.

As mentioned in Section 3, a value close to zero for ρ translates in a poorly estimation of the end-member profiles due to the low constraint on the volume of the simplex. A high value of $\boldsymbol{\rho}$ leads to singularity problems when solving for the inverse matrix

$$\left(\mathcal{A}\mathcal{A}^T + \rho\mathbf{O}\right)^{-1} \tag{11}$$

inside the closed form solution from equation (9). In addition, estimation of the abundances is worse when ρ has a high value. This is an expected result since a strong constraint in the distance between the end-member profiles, will lead to estimate similar end-members (closer vertices).

Now that the regularization parameter ρ is correctly characterized, along with the tolerance parameter ϵ and the prior information on the number of components N, the BEAE algorithm is fully automated. However, different applications will surely need a custom value for ρ. Nonetheless, it is expected to have a global value that minimizes the PRE, as in Figs. 4 and 5. Hence during the implementation of the BEAE, the optimal value of ρ has to be tuned.

Further research is required regarding the identification of m-FLIM end-members extracted by BEAE, which is a challenging problem due to high overlapping of the auto-fluorescence end-members [13]. Nevertheless, an intensity decays library is needed for reference and is under construction. Finally, only a few ex-vivo samples have been analysed using the BEAE algorithm. Future research is focused in providing more evidence of the validation of BEAE with non-synthetic samples.

Acknowledgements

The authors thank the support of PROMEP through grant F-PROMEP-39/REV-03, SEP-23-005. Omar Gutierrez-Navarro would like to acknowledge financial support by the Fulbright Mexico Commission (COMEXUS) through grant # 68120599.

[1] H. Gerritsen, A. Agronskaia, A. Bader, A. Esposito, Chapter 3 time domain flim: Theory, instrumentation, and data analysis, in: T. Gadella (Ed.), Fret and Flim Techniques, Vol. 33 of Laboratory Techniques in Biochemistry and Molecular Biology, Elsevier, 2009, pp. 95 – 132. doi:10.1016/S0075-7535(08)00003-X.
URL http://www.sciencedirect.com/science/article/pii/S007575350800003X

[2] R. Clegg, A. Periasamy, Flim applications in the biomedical sciences, in: FLIM Microscopy in Biology and Medicine, Chapman and Hall/CRC, 2009, pp. 385–400–.
[3] N. Anthony, K. Berland, P. Guo, Principles of fluorescence for quantitative fluorescence microscopy, in: FLIM Microscopy in Biology and Medicine, Chapman and Hall/CRC, 2009, pp. 35–63–.
[4] S. Schlachter, S. Schwedler, A. Esposito, G. K. Schierle, G. Moggridge, C. Kaminski, A method to unmix multiple fluorophores in microscopy images with minimal a priori information, Optics Express 17.
[5] A.-S. Montcuquet, L. Herve and, F. Navarro, J.-M. Dinten, J. Mars, In vivo fluorescence spectra unmixing and autofluorescence removal by sparse nonnegative matrix factorization, IEEE Transactions on Biomedical Engineering 58 (9) (2011) 2554 –2565. doi:10.1109/TBME.2011.2159382.
[6] M. B. Lopes, J.-C. Wolff, J. M. Bioucas-Dias, M. A. T. Figueiredo, Near-infrared hyperspectral unmixing based on a minimum volume criterion for fast and accurate chemometric characterization of counterfeit tablets, Analytical Chemistry 82 (4) (2010) 1462–1469, pMID: 20095581. arXiv:http://pubs.acs.org/doi/pdf/10.1021/ac902569e, doi:10.1021/ac902569e.
URL http://pubs.acs.org/doi/abs/10.1021/ac902569e
[7] H. Xu, B. W. Rice, In-vivo fluorescence imaging with a multivariate curve resolution spectral unmixing technique, Journal of Biomedical Optics 14, 064011.
[8] J. R. Lakowicz, Principles of Fluorescence Spectroscopy, Springer, 2006.
[9] J. R. L. Chris D. Geddes, Topics in Fluorescence Spectroscopy Volume 11 - Glucose Sensing, Springer, 2006.
[10] A. Plaza, G. Martn, J. Plaza, M. Zortea, S. Snchez, Recent developments in endmember extraction and spectral unmixing, in: R. I. Hammoud, L. B. Wolff, S. Prasad, L. M. Bruce, J. Chanussot (Eds.), Optical Remote Sensing, Vol. 3 of Augmented Vision and Reality, Springer Berlin Heidelberg, 2011, pp. 235–267.
[11] N. Keshava, J. F. Mustard, Spectral unmixing, IEEE Signal Processing Magazine 19 no. 1 (2002) pp. 44–57.
[12] D. M. Rogge, B. Rivard, J. Zhang, A. Sanchez, J. Harris, J. Feng, Integration of spatialspectral information for the improved extraction of endmembers, Remote Sensing of Environment 110 (3) (2007) 287–303.
URL http://linkinghub.elsevier.com/retrieve/pii/S0034425707000934
[13] O. Gutierrez-Navarro, D. U. Campos-Delgado, E. R. Arce-Santana, D. U. Campos-Delgado, M. O. Mendez, J. Jo, Blind endmember and abundance extraction for multi-spectral fluorescence lifetime imaging microscopy data, Submitted to IEEE Transactions on Information Technology in Biomedicine, October 2012.
[14] O. Gutierrez-Navarro, D. U. Campos-Delgado, E. R. Arce-Santana, D. U. Campos-Delgado, M. O. Mendez, J. Jo, A fully constrained optimization method for time-resolved multi-spectral fluorescence lifetime imaging microscopy data unmixing, Submitted to IEEE Transactions on Biomedical Engineering, July 2012.
[15] F. W. Young, J. de Leeuw, Y. Takane, Regression with qualitative and quantitative variables: An alternating least squares method with optimal features, Psychometrika 41 (1976) 505–526.
[16] S. Shrestha, B. E. Applegate, J. Park, X. Xiao, P. Pande, J. A. Jo, High-speed multispectral fluorescence lifetime imaging implementation for in vivo applications, Opt. Lett. 35 (15) (2010) 2558–2560. doi:10.1364/OL.35.002558.
[17] M. Berman, H. Kiiveri, R. Lagerstrom, A. Ernst, R. Dunne, J. Huntington, Ice: a statistical approach to identifying endmembers in hyperspectral images, IEEE Transactions on Geoscience and Remote Sensing 42 (10) (2004) 2085 – 2095. doi:10.1109/TGRS.2004.835299.
[18] M. Craig, Minimum volume transforms for remotely sensed data, IEEE Transactions on Geoscience and Remote Sensing (1994) pp. 542–552.
[19] J. Park, P. Pande, S. Shrestha, F. Clubb, B. E. Applegate, J. A. Jo, Biochemical characterization of atherosclerotic plaques by endogenous multispectral fluorescence lifetime imaging microscopy, Atherosclerosis 220 (2) (2012) 394 – 401. doi:10.1016/j.atherosclerosis.2011.10.034.